FBP and the interior problem in 2D tomography

Anne Bilgot*, Laurent Desbat* and Valérie Perrier†

* UJF-Grenoble 1 - CNRS, TIMC-IMAG UMR 5525, Grenoble, F-38041, France. Email: Laurent.Desbat@imag.fr

† Grenoble INP - CNRS, LJK UMR 5224, Grenoble, F-38041, France. Email: Valerie.Perrier@imag.fr

***Abstract*—We consider the Filtered Back Projection reconstruction method in the case of interior data in Computerized Tomography. In this framework we prove that the difference between the FBP reconstruction and the measured function is a continuous function. This demonstrates that the FBP reconstruction contains the discontinuities of the measured image. Thus FBP can be considered as a local reconstruction method in CT. We show numerical experiments on both simulated and real data.**

I. Introduction and Notations

The interior problem, also known as the interior Radon transform inversion, is a particular case of 2D local tomography: it refers to the situation where only truncated data, and more precisely only X-Ray projections through a central region of a larger one, are available. It is known that the densities in this central region cannot be recovered, but that the discontinuities, *in some sense*, can be identified. Thus, surfaces of discontinuity between anatomical structures are theoretically accessible [1]–[4]. This problem occurs in particular in interventional reconstruction of tomographic sections: indeed, in the operating room, conventional CT-scanners can be used, but this technique is too expensive for a widespread use, and not satisfactory as regards ergonomy and dose. An alternative consists in *fluoroscopic-based reconstruction*, for which 2D X-Ray projection data are acquired using a C-Arm; this X-Ray imaging device is conventional in the operating room and much more ergonomic than a CT scanner [5], [6]. Furthermore, it can nowadays be equipped with a distortion-free flat panel digital X-Ray detector. A drawback of this approach lies in the size of the detectors currently manufactured: they are likely to be not wide enough to collect the whole cross section of a patient lying at the isocenter of the C-Arm. This data truncation prevents from applying conventional CT-reconstruction techniques. Existing fluoroscopic-based reconstruction devices only enable to handle *exactly* small section structures, such as wrists or ankles [7]. Recent results yield analytic 2D reconstructions dealing with some trans-axial truncations [8], [9]. However, the interior problem still motivates the search for *local* algorithms, so as to ensure, at least, that location of discontinuities is properly reconstructed.

Filtered backprojection method is the conventional inversion algorithm in case of global data. In case of local data, it is usually not considered as a valuable method, for it relies on the ramp filter: this filter is not compactly-supported and thus, its application requires the knowledge of all projections. However, it is also usually known that in practice FBP method supplies satisfactory images of discontinuities. The goal of this paper is to give justification to this experimental statement, and to give elements to assess efficiency of FBP algorithm for the interior problem. In section II we prove (and it is the main result of our paper) that, as well as more sophisticated methods, FBP algorithm ensures that the difference between the original and reconstructed functions is a continuous function. In section III we illustrate this result on some images (phantom and real data). Nevertheless, in section IV, we point up examples showing strong dependencies of the reconstruction on exterior structures.

A. Filtered Backprojection Method

We first introduce some notations and classical formulas: let $\mathbb{S}^1$ denotes the unit circle in $\mathbb{R}^2$; the Radon Transform of $f \in \mathbb{L}^1(\mathbb{R}^2)$ is defined by, $\forall(\mathbf{\Theta}, s) \in \mathbb{S}^1 \times \mathbb{R}$,

$$\mathcal{R}_\theta f(s) = \mathcal{R}f(\mathbf{\Theta}, s) = \int_{\{\mathbf{x}\in\mathbb{R}^2 | \mathbf{x}\cdot\mathbf{\Theta}=s\}} f(\mathbf{x})d\mathbf{x}$$

where "$\cdot$" is the euclidean inner product, $\theta \in [0, 2\pi[$, $\mathbf{\Theta} = (\cos\theta, \sin\theta)$. In the following, we suppose that f is compactly-supported within the unit disk $\mathbf{\Omega}$ $\mathbb{R}^2$ ($f(\mathbf{x}) = 0$ if $||\mathbf{x}|| \geq 1$). The Radon transform inversion is obtained from the projection-slice theorem

$$\forall\omega \in \mathbb{R}, \widehat{\mathcal{R}_\theta f}(\omega) = \sqrt{2\pi}\widehat{f}(\omega\mathbf{\Theta}),$$

where $\widehat{\mathcal{R}_\theta f}$ and $\widehat{f}$ are respectively the 1D and 2D Fourier transforms of $\mathcal{R}_\theta f$ and f, and where for all $n \in \mathbb{N}^*$, the Fourier Transform of $f \in \mathbb{L}^1(\mathbb{R}^n)$ is normalized in the following way: for $\mathbf{k} \in \mathbb{R}^n$,

$$\hat{f}(\mathbf{k}) = \frac{1}{\sqrt{2\pi}^n} \int_{\mathbb{R}^n} f(\mathbf{x}) e^{-i\mathbf{x}\cdot\mathbf{k}} d\mathbf{k}$$

This leads to the well-known filtered backprojection inversion formula [2] (FBP inversion method in the following):

$$f(\mathbf{x}) = \frac{1}{\sqrt{2\pi}^3} \int_0^\pi \int_{\mathbb{R}} \widehat{\mathcal{R}_\theta f}(\omega)|\omega| e^{i\omega\mathbf{x}\cdot\mathbf{\Theta}} d\omega d\theta \qquad (1)$$

which can be reformulated in the following way:

$$f(\mathbf{x}) = \frac{1}{\sqrt{2\pi}^3} \int_0^\pi (\mathrm{ramp} * \mathcal{R}_\theta f)(\mathbf{x}\cdot\mathbf{\Theta}) d\theta \qquad (2)$$

where ramp denotes the 1D ramp filter:

$$\begin{aligned}(\text{ramp} * \mathcal{R}_\theta f)(s) &= \sqrt{\frac{2}{\pi}} \left(\text{vp}\left(\frac{1}{s}\right) * \partial_s \mathcal{R}_\theta f \right)(s) \\ &= \sqrt{\frac{2}{\pi}} \lim_{\epsilon \to 0^+} \int_{[-1;s-\epsilon]\cup[s+\epsilon;1]} \frac{\partial_s \mathcal{R}_\theta f(u)}{s-u} du.\end{aligned}$$

Reamark that $\widehat{\text{ramp}}(\omega) = |\omega|$. Finally, Eq. (1) reads:

$$f(\mathbf{x}) = \frac{1}{2\pi^2} \int_0^\pi \lim_{\epsilon \to 0^+} \int_{[-1;\mathbf{x}\cdot\mathbf{\Theta}-\epsilon]\cup[\mathbf{x}\cdot\mathbf{\Theta}+\epsilon;1]} \frac{\partial_s \mathcal{R}_\theta f(u)}{\mathbf{x}\cdot\mathbf{\Theta} - u} du d\theta$$

B. The interior problem

Let a $(0 < a < 1)$ be the radius of the Region Of Interest (ROI). The ROI is assumed to be here also the region of exposure. The interior problem is defined as follows: using only the interior components of the Radon transform, namely

$$(\mathcal{R}f)_{\text{int}} = \left\{ \mathcal{R}f(\mathbf{\Theta}, s); \mathbf{\Theta} \in \mathbb{S}^1, s \in [-a, a] \right\},$$

is it possible to reconstruct the values of f inside the ROI? The response is well known [2], [10], [11]: it is not possible, and more precisely, the interior problem is ill-posed in the sense that it is not uniquely solvable. In order to give briefly further intuition about this well-known property, let us suppose that we apply the inverse of the Radon transform $\mathcal{R}^{-1}$ to the interior data only, in order to estimate f in the ROI. The set of non-considered data in the interior problem will be denoted by:

$$(\mathcal{R}f)_{\text{ext}} := \left\{ \mathcal{R}f(\mathbf{\Theta}, s); \mathbf{\Theta} \in \mathbb{S}^1, |s| > a \right\}.$$

As illustrated in Fig. 1:

- left: when a structure with support included in the ROI is considered, the Radon transform has only interior components ($\mathcal{R}f = (\mathcal{R}f)_{\text{int}}$);
- right: when a structure with support outside the ROI is considered, the Radon transform has exterior components ($(\mathcal{R}f)_{\text{ext}}$), *but also* interior components ($(\mathcal{R}f)_{\text{int}} \neq \mathbf{0}$).

Therefore, for a function $f = f_{\text{int\_2D}} + f_{\text{ext\_2D}}$ with structures both in the ROI ($f_{\text{int\_2D}}(\mathbf{x}) := f(\mathbf{x})\chi_{\{|\mathbf{x}|\leq a\}}(\mathbf{x})$) and outside the ROI ($f_{\text{ext\_2D}} := f - f_{\text{int\_2D}}$), the available data in the interior problem are made of two components:

$$(\mathcal{R}f)_{\text{int}} = \mathcal{R}f_{\text{int\_2D}} + (\mathcal{R}f_{\text{ext\_2D}})_{\text{int}}$$

and the inversion of these data using global (linear) inversion operator, denoted here by $\mathcal{R}^{-1}$, leads to the reconstruction of the following function (this inversion operator is linear) :

$$\begin{aligned} f_{\text{loc}} &= \mathcal{R}^{-1}\left((\mathcal{R}f)_{\text{int}}\right) \\ &= \mathcal{R}^{-1}\left(\mathcal{R}f_{\text{int\_2D}}\right) + \mathcal{R}^{-1}\left((\mathcal{R}f_{\text{ext\_2D}})_{\text{int}}\right) \\ &= f_{\text{int\_2D}} + \mathcal{R}^{-1}\left((\mathcal{R}f_{\text{ext\_2D}})_{\text{int}}\right)\end{aligned}$$

Thus, in the ROI, the initial function $f_{\text{int\_2D}}$ is corrupted by $\mathcal{R}^{-1}\left((\mathcal{R}f_{\text{ext\_2D}})_{\text{int}}\right)$.This bias is present in all even dimensions and observable in reconstructions. The existence of this bias is sufficient to motivate the search for other reconstruction methods, such as local methods.

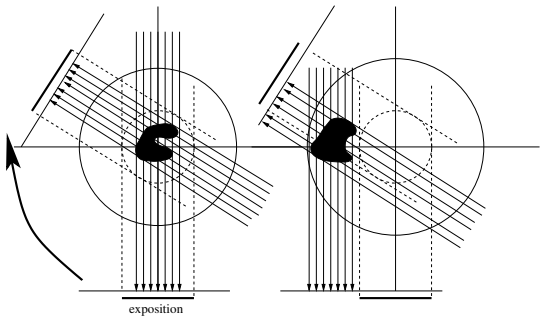

Fig. 1. Interior problem in 2D parallel geometry: on the left, the object is entirely included in the ROI (dashed circle): the Radon transform reduces to interior data. On the right, the object lies in the exterior of the ROI: the Radon transform data have not only exterior contributions, but also interior contributions.

C. Local methods for the interior problem

The purpose of local methods dedicated to the interior problem is the following: they aim at "reconstructing discontinuities" in the ROI, in the sense: to reconstruct a function with discontinuities exactly located as in the initial function, and sometimes, even with the same jumps. The legitimacy of such a purpose relies on a theorem of micro-local analysis, established by Quinto [1]: this theorem links the singular supports (discontinuity curves) of f and $\mathcal{R}f$ and more precisely the wavefronts of f and $\mathcal{R}f$ (which additionally give the normal directions) , see [1] for details.

The literature provides several approaches to the interior problem:

- Λ-*Tomography* (see for instance [12]) where one reconstructs Λf instead of f (the pseudo-differential operator Λ, defined by $\widehat{\Lambda f}(\mathbf{k}) = |\mathbf{k}|\hat{f}(\mathbf{k})$, is locally recoverable, and known to preserve the discontinuities).
- *Pseudolocal Tomography* [3], where one copes with the non-locality of the ramp filter by truncating it in the direct domain. We detail this method below.
- *Geometrical approaches* [13], which consist in detecting the discontinuities in the sinogram, and then deducing the discontinuities in the image; in practice, singularities are highly difficult to detect in the data.
- *Wavelet based-methods* where separable [14], [15] or non separable [16] multiresolution analysis are recovered using local data: the 2D wavelet transform of a function f can be computed from a 1D wavelet transform of its Radon transform $\mathcal{R}f$; it can be seen as a generalization of the FBP algorithm. The locality of the wavelet filtering enables to reconstruct wavelet coefficients of the function f *up to a given scale*, according to the range of availability of data [17], [18]; fine details, and therefore discontinuities, are thus visible. A generalization of wavelet based-methods, relying on theoretical work by Holschneider [19], is also applied to the interior problem in [20].
- *Identification of the directional Hilbert transform* of a function f according to the Hilbert transform of the pro-

jections, see [8], [9], [21]–[23]. These methods enable the reconstruction of f on lines (or half lines) crossing a ROI, but are not suited to the interior problem (considered ROI can not be interior disks, except if *a priori* knowledge is given [21]). ROI reconstructions from truncated data can also be performed with *the virtual fan-beam projection method* thanks to links that can be established between the Hilbert transform of the fan beam projections and the Hilbert transform of parallel projections, see [24]: however, this can not solve the interior problem. See [25] for an excellent review.

In contrast to these methods, FBP is traditionally not considered as a valuable approach for the interior problem, because it relies on the ramp filter (2): this filter is non-local and thus, its application requires the knowledge of all projection. In the following, we prove that although these arguments are true, FBP is nevertheless a local method, in the sense of that, as pseudo-local tomography does, it enables discontinuity reconstruction.

II. Truncated formulas for truncated data

In the following the filtered backprojection applied to interior data is called *Truncated Filtered Backprojection* or TFBP.

A. Pseudo-local tomography

This method has been designed by A. Katsevitch and A. Ramm [3]. The idea consists in truncating the ramp filter in the direct domain so as to filter local data with a filter restricted to an interval $[-d,d]$ (where $d>0$ and for treatment of local data $d << a$); thus, instead of reconstructing f by

$$\begin{aligned} f(\mathbf{x}) &= \frac{1}{2\pi^2}\int_0^\pi \lim_{\epsilon\to 0^+}\left(\int_{-1}^{\mathbf{x}\cdot\mathbf{\Theta}-\epsilon}\frac{\partial_s\mathcal{R}_\theta f(s)}{\mathbf{x}\cdot\mathbf{\Theta}-s}ds\right.\\ &+ \left.\int_{\mathbf{x}\cdot\mathbf{\Theta}+\epsilon}^{1}\frac{\partial_s\mathcal{R}_\theta f(s)}{\mathbf{x}\cdot\mathbf{\Theta}-s}ds\right)d\theta \end{aligned}$$

one reconstructs the function f_d, defined by:

$$\begin{aligned} f_d(\mathbf{x}) &= \frac{1}{2\pi^2}\int_0^\pi \lim_{\epsilon\to 0^+}\left(\int_{\mathbf{x}\cdot\mathbf{\Theta}-d}^{\mathbf{x}\cdot\mathbf{\Theta}-\epsilon}\frac{\partial_s\mathcal{R}_\theta f(s)}{\mathbf{x}\cdot\mathbf{\Theta}-s}ds\right.\\ &+ \left.\int_{\mathbf{x}\cdot\mathbf{\Theta}+\epsilon}^{\mathbf{x}\cdot\mathbf{\Theta}+d}\frac{\partial_s\mathcal{R}_\theta f(s)}{\mathbf{x}\cdot\mathbf{\Theta}-s}ds\right)d\theta \end{aligned}$$

The reconstruction of f can be made locally, in the sense that the reconstruction of f at point $\mathbf{x}$ only requires the knowledge of $\mathcal{R}f$ across the disk centered at $\mathbf{x}$ and radius d. To identify the information on f present in f_d, the authors introduce the function f_d^{C}, difference between f_d and the reference function f, defined by: $f_d^{\mathrm{C}}(\mathbf{x}) = f(\mathbf{x}) - f_d(\mathbf{x})$ and they prove the following key-theorem.

Theorem 1 (Pseudo-local tomography [3])**.** *For all $d>0$, the function f_d^{C} is continuous in the direct domain.*

It follows that the discontinuities of f_d are exactly the same as those of f (location as well as amplitude). The proof of this result is based on continuity properties of integrals with parameters, and can be found in [3].

B. Truncated FBP

We introduce the following reconstructed function, obtained by application of global FBP reconstruction method on interior data: for $0<a\leq 1$,

$$\begin{aligned} f^a_{\mathrm{TFBP}}(\mathbf{x}) &= \frac{1}{2\pi^2}\int_0^\pi \lim_{\epsilon\to 0^+}\left(\int_{-a}^{\mathbf{x}\cdot\mathbf{\Theta}-\epsilon}\frac{\partial_s\mathcal{R}_\theta f(s)}{\mathbf{x}\cdot\mathbf{\Theta}-s}ds\right.\\ &+ \left.\int_{\mathbf{x}\cdot\mathbf{\Theta}+\epsilon}^{a}\frac{\partial_s\mathcal{R}_\theta f(s)}{\mathbf{x}\cdot\mathbf{\Theta}-s}ds\right)d\theta \end{aligned}$$

A question then naturally follows : what can be learned about f according to f^a_{TFBP}? In [2], Natterer gives an answer to a very close question : in the framework of C^∞-functions, he proposes to complete the interior data by consistency into the whole domain; applying FBP algorithm to these completed data, he then proves that the reconstructed function only differs from the original one up to an essentially constant function.

Giving another point of view, we introduce the difference between the original function f and f^a_{TFBP}:

$$\begin{aligned} \left(f^a_{\mathrm{TFBP}}\right)^{\mathrm{C}}(\mathbf{x}) &= f(\mathbf{x}) - f^a_{\mathrm{TFBP}}(\mathbf{x})\\ &= \frac{1}{2\pi^2}\int_0^\pi\int_{-1}^{-a}\frac{\partial_s\mathcal{R}_\theta f(s)}{\mathbf{x}\cdot\mathbf{\Theta}-s}ds\\ &+ \int_a^1\frac{\partial_s\mathcal{R}_\theta f(s)}{\mathbf{x}\cdot\mathbf{\Theta}-s}dsd\theta \end{aligned} \tag{3}$$

We prove in the following the main result of this paper: just as in pseudo-local tomography, the difference $\left(f^a_{\mathrm{TFBP}}\right)^{\mathrm{C}}$ is a continuous function in the ROI; therefore the discontinuities of f^a_{TFBP} are exactly the same as the discontinuities of f within the ROI. A close result is obtained independently in [26] with different and stronger assumptions (the exterior data are supposed to be smooth), using different arguments.

Theorem 2 (Truncated Filtered BackProjection)**.** *For all $0<a\leq 1$, the function $\left(f^a_{\mathrm{TFBP}}\right)^{\mathrm{C}}$ defined in (3) is continuous in the disk $\{\mathbf{x}\in\mathbb{R}^2;|\mathbf{x}|\leq r\}$, for all r such that $0<r<a$.*

Proof: Let D_r denotes the closed disk of radius r, strictly included in the region of exposure, (*i.e.*, $r<a$). First, remark that for all $f\in\mathbb{L}^2(\mathbf{\Omega})$, (3) is well-defined; indeed, if $f\in\mathbb{L}^2(\mathbf{\Omega})$, then, for all $\theta\in[0;\pi]$, $\mathcal{R}_\theta f\in\mathbb{H}^{\frac{1}{2}}(]-1;1[)$ (see [2] for a proof of this regularization result) and $\partial_s\mathcal{R}_\theta f\in\mathbb{H}^{-\frac{1}{2}}(]-1;1[)$ (this point, as well as following assertions in this paragraph, can be proven thanks to the relation between the Fourier transforms of these two functions). Eq. (3) then rewrites, for all $\mathbf{x}$ in D_r:

$$\begin{aligned} \left(f^a_{\mathrm{TFBP}}\right)^{\mathrm{C}}(\mathbf{x}) &= \frac{1}{2\pi^2}\mathcal{R}^{\#}\left(\mathrm{vp}\left(\frac{1}{s}\right)*\left(\chi_{[-1,-a]}\ \partial_s\mathcal{R}_\theta f\right)\right)(\mathbf{x})\\ &+ \frac{1}{2\pi^2}\mathcal{R}^{\#}\left(\mathrm{vp}\left(\frac{1}{s}\right)*\left(\chi_{[a,1]}\ \partial_s\mathcal{R}_\theta f\right)\right)(\mathbf{x}) \end{aligned}$$

where $\mathcal{R}^{\#}$ denotes the backprojection operator, defined by :

$$\mathcal{R}^{\#}g(\mathbf{x}) = \int_0^\pi g(\mathbf{\Theta},\mathbf{x}\cdot\mathbf{\Theta})d\theta$$

and where χ_X is the characteristic function of interval X. Since $\chi_{[a,1]}\ \partial_s \mathcal{R}_\theta f$ belongs also to $\mathbb{H}^{-\frac{1}{2}}(]-1;1[)$, then $\mathrm{vp}\left(\frac{1}{s}\right)*\left(\chi_{[a,1]}\ \partial_s \mathcal{R}_\theta f\right)$ remains in $\mathbb{H}^{-\frac{1}{2}}(]-1;1[)$, which leads finally to $\mathcal{R}^{\#}\left(\mathrm{vp}\left(\frac{1}{s}\right)*\left(\chi_{[a,1]}\ \partial_s \mathcal{R}_\theta f\right)\right) \in \mathbb{L}^2(\mathbf{\Omega})$ (and idem on interval $[-1,-a]$). Thus, (3) is well-defined.

By an integration by parts on (3) (we recall that $\mathcal{R}_\theta f(-1) = \mathcal{R}_\theta f(1) = 0$ for all θ), we get, for all $\mathbf{x}$ in D_r,

$$\begin{aligned}
&\left(f^a_{\mathrm{TFBP}}\right)^{\mathrm{C}}(\mathbf{x}) \\
= &\frac{1}{2\pi^2}\int_0^\pi \left(\left[\frac{\mathcal{R}_\theta f(s)}{\mathbf{x}\cdot\mathbf{\Theta}-s}\right]_{-1}^{-a} + \int_{-1}^{-a} \frac{\mathcal{R}_\theta f(s)}{(\mathbf{x}\cdot\mathbf{\Theta}-s)^2} ds \right. \\
+ &\left. \left[\frac{\mathcal{R}_\theta f(s)}{\mathbf{x}\cdot\mathbf{\Theta}-s}\right]_{a}^{1} + \int_{a}^{1} \frac{\mathcal{R}_\theta f(s)}{(\mathbf{x}\cdot\mathbf{\Theta}-s)^2} ds \right) d\theta \\
= &\frac{1}{2\pi^2}\left[\int_0^\pi \left(\frac{\mathcal{R}_\theta f(-a)}{\mathbf{x}\cdot\mathbf{\Theta}+a} - \frac{\mathcal{R}_\theta f(a)}{\mathbf{x}\cdot\mathbf{\Theta}-a}\right) d\theta \right. \qquad (4) \\
+ &\left. \int_0^\pi \left(\int_{-1}^{-a} \frac{\mathcal{R}_\theta f(s)}{(\mathbf{x}\cdot\mathbf{\Theta}-s)^2} ds + \int_a^1 \frac{\mathcal{R}_\theta f(s)}{(\mathbf{x}\cdot\mathbf{\Theta}-s)^2} ds \right) d\theta \right]
\end{aligned}$$

In the following, we check that the conditions that are required to apply the results about continuity of integrals with parameters are fulfilled, so as to prove that $\left(f^a_{\mathrm{TFBP}}\right)^{\mathrm{C}}$ is continuous at point $\mathbf{x} \in D_r$.

For the first integral in (4), we have:

- for all $\theta \in [0,\pi[$, the functions $\mathbf{x} \mapsto \dfrac{\mathcal{R}_\theta f(-a)}{\mathbf{x}\cdot\mathbf{\Theta}+a}$ and $\mathbf{x} \mapsto \dfrac{\mathcal{R}_\theta f(a)}{\mathbf{x}\cdot\mathbf{\Theta}-a}$ are continuous in D_r (because for each θ, $\mathbf{x}\cdot\mathbf{\Theta} \pm a$ never vanishes, as $|\mathbf{x}\cdot\mathbf{\Theta}| \leq |\mathbf{x}| \leq r < a$);
- moreover for all $\mathbf{x} \in D_r$, $-r < \mathbf{x}\cdot\mathbf{\Theta} < r$, we have $0 < a - r < \mathbf{x}\cdot\mathbf{\Theta} + a$, and then
$$\left|\frac{\mathcal{R}_\theta f(-a)}{\mathbf{x}\cdot\mathbf{\Theta}+a}\right| \leq \frac{|\mathcal{R}_\theta f(-a)|}{a-r}$$
which is a function (of θ), integrable on $[0,\pi]$. A similar argument can be used for the function $\mathbf{x} \mapsto \dfrac{\mathcal{R}_\theta f(a)}{\mathbf{x}\cdot\mathbf{\Theta}-a}$; it follows that the first integral of (4) is a continuous function of $\mathbf{x}$ in D_r.

For the second integral in (4), we have:

- for each couple $(\theta,s) \in [0,\pi]\times[-1,-a]$ (resp. each couple $(\theta,s) \in [0,\pi]\times[a,1]$), the function $\mathbf{x} \mapsto \dfrac{\mathcal{R}_\theta f(s)}{(\mathbf{x}\cdot\mathbf{\Theta}-s)^2}$ is continuous in D_r (because $\mathbf{x}\cdot\mathbf{\Theta} - s$ never vanishes);
- moreover for all $\mathbf{x} \in D_r$, for all $(\theta,s) \in [0,\pi]\times[-1,-a]$,
$$0 < -r + a \leq -r - s \leq \mathbf{x}\cdot\mathbf{\Theta} - s$$
therefore
$$\left|\frac{\mathcal{R}_\theta f(s)}{(\mathbf{x}\cdot\mathbf{\Theta}-s)^2}\right| \leq \left|\frac{\mathcal{R}_\theta f(s)}{(a-r)^2}\right|$$
the r.h.s. being a function of (θ,s), integrable on $[0,\pi]\times[-1,-a]$.

A similar proof can be made for the third integral of (4): the sum of the second and the third integral is thus a continuous function of $\mathbf{x}$ in D_r.

III. Numerical experiments

A. Example 1: Shepp and Logan phantom

We first show reconstruction results obtained by TFBP applied to Shepp and Logan phantom (displayed on the first line of figure 2, with a zoom-in on the ROI displayed on the right). We fix $0 < a \leq 1$ and simulate the truncated Radon transform of the phantom:

$$\forall(\mathbf{\Theta},s) \in \mathbb{S}^1 \times [-1,1],\ g(\mathbf{\Theta},s) = \begin{cases} \mathcal{R}f(\Theta,s) \text{ if } |s| \leq a \\ 0 \text{ else} \end{cases} \qquad (5)$$

The results are displayed on the left of figure 2 (second and third line). The initial image is the square $[-1,1]^2$ sampled on 256^2 pixels. The radius of the ROI is $a = 0.25$, and the data are acquired on 450 equiangular projections on $[0,\pi[$, each of them sampled with a step $\frac{2}{256}$.

There is only a bias, roughly constant in the ROI, between the phantom and the reconstruction, and as Theorem 2 asserts, the discontinuities of the phantom are clearly visible in the reconstruction. Although this reconstruction is satisfactory if one aims at localizing discontinuities, it is common in local tomography literature to use a procedure to reduce artifacts at the ROI boundary [14], [16]: it consists in erasing discontinuities at the truncated sinogram boundary, by extending by continuity interior data in a constant way:

$$\forall(\Theta,s) \in \mathbb{S}^1\times[-1,1],\ g(\mathbf{\Theta},s) = \begin{cases} \mathcal{R}f(\mathbf{\Theta},s) \text{ if } |s| \leq a \\ \mathcal{R}f(\mathbf{\Theta},a) \text{ if } s > a \\ \mathcal{R}f(\mathbf{\Theta},-a) \text{ if } s < -a \end{cases} \qquad (6)$$

Theorem 2 is still valid: discontinuities of the reconstruction are the same than the ones of the phantom. The results are displayed on the right of figure 2 (second and third line). The artifacts in the reconstruction are clearly reduced at the borders at the ROI boundary, as well as the amplitude of the bias in the ROI. Discontinuities are still clearly visible, but the visual similarity (as regards gray levels) with the phantom is much improved: local reconstruction really "looks like" the phantom.

B. Example 2: Real data

We have then applied TFBP technique on real data (human trabecular bone sample), kindly provided by F. Peyrin [27], and acquired on the medical line of ESRF Grenoble (European Synchrotron Radiation Facility). The projections were sampled on 1024 pixels of 15 μm, for 900 directions. The length of the medical line is 145 m, thus we consider that parallel beam conditions are fulfilled. Results are displayed on figure 3. They are fully satisfactory: even small details in the ROI are well localized in the reconstruction.

IV. Discussion

Both previous examples tend to show that TFBP is a very satisfactory method for the interior problem. In order to assess the range of efficiency of TFBP, we have tried to build phantoms for which TBFP behavior is less convincing. As explained in paragraph I-B, the bias created in the ROI in case

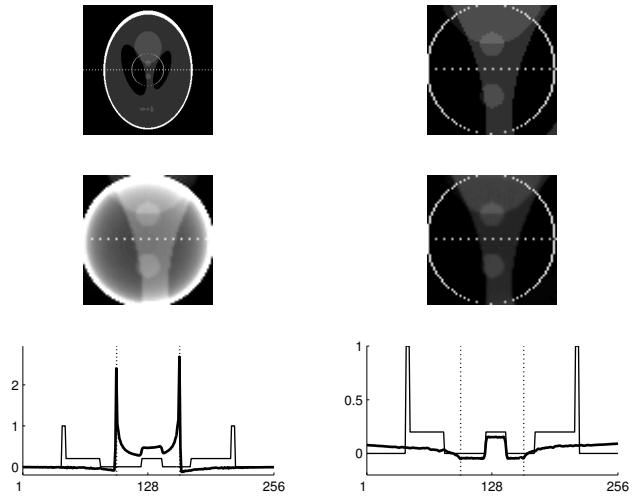

Fig. 2. Results of TFBP applied on interior data on Shepp and Logan phantom. First line, the phantom, with, on the right, a zoom-in on the ROI. Second and third line, on the left: reconstructions from *raw* local data (exterior data are zero), and on the right, reconstructions from data extended by continuity. Third line, in both cases, a zoom-in on the ROI of the reconstruction and comparisons between the phantom and the reconstruction horizontal cross-sections are displayed (the darker line stands for the reconstruction). Note that the values of the jumps are well estimated.

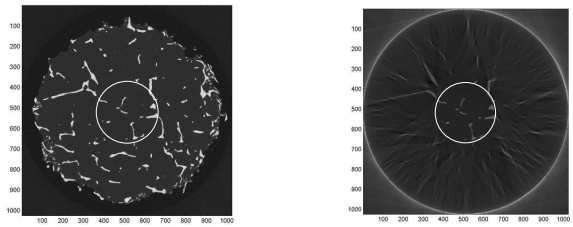

Fig. 3. FBP-reconstruction results on real data (human trabecular bone sample data, kindly provided by F. Peyrin, ESRF Grenoble [27]). These data were acquired at ESRF (European Synchrotron Radiation Facility) on the medical line. The projections were sampled on 1024 pixels of 15 μm, for 900 directions. The similarity between the reconstruction from global data (left) and local data (right) is fully satisfactory in the ROI, even for small details.

of local data comes from exterior structures: we have thus tried to compare influences of several kinds of exterior structures, by designing phantoms where only exterior structures are present. Results are displayed in figure 4 (interior data have been extended by continuity). It thus appears that in case of Shepp and Logan phantom, the different contributions of external data tend to compensate in the ROI, thus creating a bias which is roughly constant, and thus leading to visually very satisfactory local reconstruction results. On the contrary, for the second and the third phantoms, we have put structures with high density, non-symmetrically distributed around the ROI. The bias implied in the ROI has no discontinuity (as theory proves), but has significant decay in the ROI (with even an inflection point in the third case). Therefore, the identification of discontinuities in the ROI is not compromised, but asymmetry is forced in the ROI. Consequently, in case of such exterior structures, two similar structures in the ROI can be reconstructed in two different ways. Such an example is given in figure 5: disks are not reconstructed with the same gray levels whether they are close to the white exterior rectangles or not. In such a case, the reconstruction image tends to show that the two structures have different densities, whereas they actually have the same.

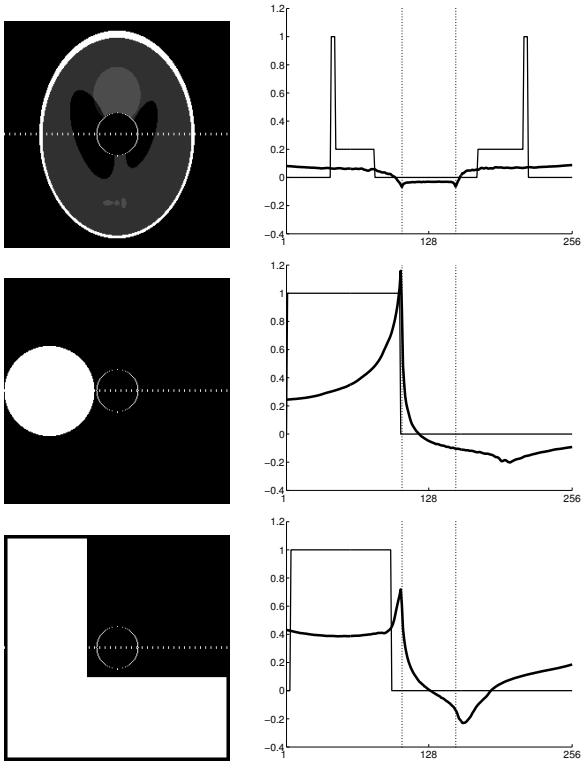

Fig. 4. Comparisons of the influence of three kinds of exterior data on the TFBP-reconstruction within the ROI. The three phantoms are displayed on the first column, and the reconstructions obtained by TFBP applied on interior data are displayed on the second one. For the Shepp and Logan phantom (first line), only a constant bias is created. In the two other cases, with high density exterior structures localized only on some sides of the ROI, the bias has significant decay across the ROI: a dis-symmetry is thus created in the ROI.

Comparison with other local methods

- TFBP is very simple: a conventional FBP algorithm can be used without any modification.
- TFBP, like Λ-tomography and pseudo-local tomography, provides a reconstructed function which has the same discontinuities as the reference function.
- TFBP has the same complexity as FBP; it is well-known that the most expensive step is the backprojection, present in all considered local methods.
- Finally, the main drawback of TFBP is its unpredictable "qualitative performance", due to its might-be dependence on exterior structures. For a given function f, other local algorithms, which implement truly local filters, reconstruct in the ROI the same function whether the sinogram is complete or not; it is not the case for TFBP.

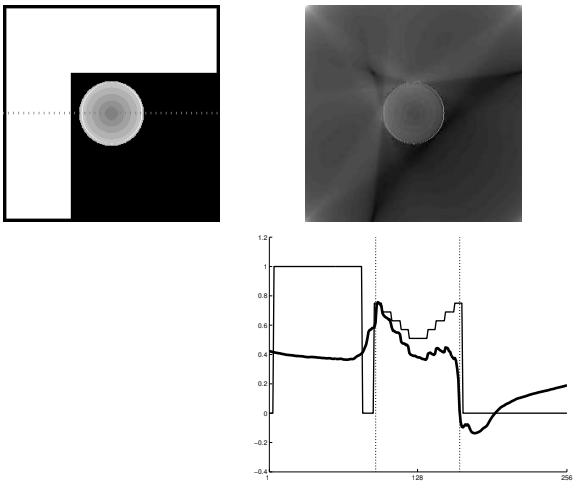

Fig. 5. An example where exterior data have influence on the TFBP-reconstruction in the ROI. The phantom is displayed in the first column, with a zoom-in on the ROI, the reconstruction obtained by TFBP in the second column, and the comparison of cross-sections in the third column. A significant asymmetry is created in the ROI by TFBP.

V. Conclusion

In this paperwork we have studied the behavior of "Truncated Filtered Backprojection" (i.e., FBP applied on interior problem data). As for pseudo-local tomography, we have proved that the difference between the reference function and the reconstructed function from TFBP is continuous on the ROI. This supplies a justification to an experimental intuition: this simple method provides with very satisfactory results if one is only interested in the location of discontinuities in the reconstruction. Furthermore, we have verified on true data that the visual similarity between FBP from complete data and TFBP from truncated interior data can be very high. Nevertheless, we have also shown on numerical experiments that TFBP method can be strongly dependent on exterior structures.

In conclusion, if not only discontinuities but also symmetry preservation is crucial in the application, other local methods should be considered. If only discontinuity localization is sufficient, the TFBP algorithm is a very simple and efficient method.

Acknowledgments

The authors would like to thank Françoise Peyrin for fruitful discussions and for providing the ESRF data.

References

[1] E. Quinto, "Singularities of the X-ray transform and limited data tomography in $\mathbf{R}^2$ and $\mathbf{R}^3$," *SIAM J. Math. Anal.*, vol. 24, pp. 1215–1225, 1993.

[2] F. Natterer, *The Mathematics of Computerized Tomography*, ser. Classics in Applied Mathematics. SIAM, 2001.

[3] A. Katsevich and A. Ramm, "Pseudolocal tomography," *SIAM Journal of Applied Mathematics*, vol. 56, no. 1, pp. 167–191, 1996.

[4] J.-P. Thirion, "Segmentation of tomographic data without image reconstruction," *IEEE Transactions on Medical Imaging*, vol. 11, no. 1, pp. 102–110, March 1992.

[5] E. Euler, S. Heining, C. Riquarts, and W. Mutschler, "C-arm-based three-dimensional navigation: a preliminary feasibility study," *Computer Aided Surgery*, pp. 35–41, 2003.

[6] M. Fleute, S. Lavalle, and L. Desbat, "Integrated approach for matching statistical shape models with intra-operative 2D and 3D data." in *MICCAI*, T. Dohi and R. Kikinis, Eds. Springer-Verlag, 2002.

[7] D. Kendoff, M. Citak, T. Hüfner, S. Chaudhary, and C. Krettek, "Current concepts and applications of computer navigation in orthopedic trauma surgery," *Central European Journal of Medicine*, vol. 2, no. 4, pp. 392–403, 2007.

[8] F. Noo, R. Clackdoyle, and J. Pack, "A two-step hilbert transform method for 2d image reconstruction," *Phys. Med. Biol.*, vol. 49, pp. 3903–23, 2004.

[9] M. Defrise, F. Noo, R. Clackdoyle, and H. Kudo, "Truncated hilbert transform and image reconstruction from limited tomographic data," *Inverse Problems*, vol. 22, pp. 1037–53, 2006.

[10] P. Maass, "The interior radon transform," *SIAM J. Appl. Math.*, vol. 52, pp. 710–724, 1992.

[11] A. K. Louis and A. Rieder, "Incomplete data problems in x-ray computerized tomography," *Numerische Mathematik*, vol. 56, pp. 371–383, 1989.

[12] A. Faridani, K. Buglione, P. Huabsomboon, O. Iancu, and J. McGrath, "Introduction to local tomography," in *Radon Transforms and Tomography*, ser. Contemporary Mathematics, E. Quinto *et al.*, Ed. American Mathematical Society, 2001, vol. 278, pp. 29–47.

[13] A. Ramm and A. Katsevich, *The Radon Transform and Local Tomography*. CRC Press, 1996.

[14] F. Rashid Farrokhi, K. Ray Liu, C. Berenstein, and D. Walnut, "Wavelet-based multiresolution local tomography," *IEEE Transactions on Image Processing*, vol. 6, no. 10, pp. 1412–1429, 1997.

[15] C. Berenstein and D. Walnut, "Wavelets and local tomography," in *Wavelets in Medicine and Biology*, Aldroubi and Unser, Eds. CRC Press, 1996, pp. 231–261.

[16] S. Bonnet, F. Peyrin, F. Turjman, and R. Prost, "Tomographic reconstruction using nonseparable wavelets," *IEEE Transactions on image processing*, vol. 9, no. 8, pp. 1445–1450, 2000.

[17] T. Olson and J. DeStefano, "Wavelet localization of the Radon transform," *IEEE Transactions on Signal Processing*, vol. 42 (8), pp. 2055–2067, 1994.

[18] A. Delaney and Y. Bresler, "Multiresolution tomographic reconstruction using wavelets," *IEEE Transactions on Image Processing*, vol. 4, no. 6, pp. 799–813, 1995.

[19] M. Holschneider, "Inverse Radon transforms through inverse wavelet transforms," *Inverse Problems*, vol. 7, pp. 853–861, 1991.

[20] A. Bilgot, "Méthodes locales d'identification de surfaces de discontinuité à partir de projections tronquées pour l'imagerie interventionnelle." Ph.D. dissertation, Université J. Fourier, Grenoble I, 2007.

[21] M. Courdurier, F. Noo, M. Defrise, and H. Kudo, "Solving the interior problem of computed tomography using *a priori* knowledge," *Inverse Problems*, vol. 24, no. 6, 2008.

[22] Y. Ye, H. Yu, W. Y., and G. Wang, "A general local reconstruction approach based on a truncated hilbert transform," *International Journal of Biomedical Imaging*, vol. Article ID 63634, 8 pages, 2007.

[23] H. Yu, Y. Ye, and G. Wang, "Interior reconstruction using the truncated hilbert transform via singular value decomposition," *Journal of X-Ray Science and Technology*, vol. 16, pp. 243–251, 2008.

[24] F. Noo, M. Defrise, R. Clackdoyle, and H. Kudo, "Image reconstruction from fan-beam projections on less than a short-scan," *Phys. Med. Biol.*, vol. 47, pp. 2525–2546, July 2002.

[25] R. Clackdoyle and M. Defrise, "Tomographic reconstruction in the 21st century," *IEEE Signal Processing Magazine*, vol. 27, no. 4, pp. 60–80, 2010.

[26] H. Yu and G. Wang, "Compressed sensing based interior tomography," *Phys. Med. Biol.*, vol. 54, pp. 2791–2805, 2009.

[27] A. L., B. V., B. O., O. C., Y. S., T. J., D. J. M., B. E., K. P. O., and P. F., "Relevance of 2d radiographic texture analysis for the assessment of 3d bone micro-architecture," *Medical Physics*, vol. 33, no. 9, pp. 3546–3556, 2006.